Final Draft

of the original manuscript

Gazenbiller, E.; Arya, V.; Reitz, R.; Engler, T.; Oechsner, M.; Höche, D.:

Statistical analysis of AA-1050 localized corrosion in anhydrous ethanol.

In: Corrosion Science. Vol. 179 (2021) 109137.

First published online by Elsevier: 17.11.2020

https://dx.doi.org/10.1016/j.corsci.2020.109137

Data-based analysis of AA-1050 localized corrosion in anhydrous ethanol

Eugen Gazenbiller Visheet Arya Rüdiger Reitz Tom Engler
Matthias Oechsner Daniel Höche

June 2, 2020

1 Introduction

Greenhouse gas emissions related to combustion of fossil fuels are regarded as the main cause of global warming. In order to reduce the dependence on non-renewable energy carriers, fuels can be blended with different percentages of bio-ethanol. Second and third generation bioethanol can be obtained from lignocellulosic waste or algal biomass, respectively, and is considered a sustainable energy source which does not compete with worldwide food supplies.[1, 2] Each country regulates the allowed amounts according to norms, e.g. DIN EN 15376 in Germany or ASTM D 4806 in the United States.[3] Nonetheless, the increased reactivity of alcohols in comparison to inert hydrocarbons can be problematic in combinations with certain materials that are used in automotive construction.

In particular, the high pitting corrosion susceptibility of aluminium alloys in ethanol containing fuels with a low water content raised the attention of materials science community in recent years.[4–13] The bulk of the publications focuses on a phenomenological description of the pitting occurrence and the effect of temperature and water and ethanol content. It can be concluded from existing research that high temperature and ethanol percentage as well as low water content increase the pitting susceptibility of aluminium alloys.[7–9] Nonetheless, the delicate balance between pit initiation and growth, the number of influencing factors and the high degree of uncertainty of experimental outcomes impedes precise quantitative conclusions towards compatibility predictions.

Calabrese *et al.* recently postulated a complete mechanism, starting from passive layer breakdown due to water loss to pit propagation on Al alloys in anhydrous ethanol at elevated temperatures.[12] Park *et al.* elaborated the effect of dissolved oxygen on the corrosiveness of E20 fuels on Al alloys and concluded that it has a passivating effect due to released water molecules upon ethanol oxidation.[6] Kruger's and Thomson's results indicate that galvanic effects do not affect the corrosion behavior of Al alloys.[7, 9]

Furthermore, although the general reaction pattern of aluminium in water-free ethanol (so called "dry corrosion", see Refs. [4–13]) is well accepted, several authors do not address or elaborate the differences between a possible chemical and electrochemical mechanism.[4, 11, 13] This is problematic because the results of often employed electrochemical methods for corrosion prediction are not directly applicable for forecasting alloy behavior for service-oriented conditions.

The concept of competing electrochemical and chemical corrosion mechanisms was introduced by Kolotyrkin and co-workers in order to explain the discrepancies between calculated and measured corrosive mass losses of iron and chromium in acidic aqueous solutions.[14] The effect was also described by Garreau for Al in ethanol electrolytes and explained with the existence of a monovalent Al-ion intermediate and subsequent competition between a chemical and electrochemical route.[15] The extent of each is mainly determined by the Al^+ stability in the particular electrolyte.

Although statistical analysis of localized corrosion is well established,[16–19] to the best of our knowledge, there are no publications which employ such methods on temperature-induced pitting in organic solvents. The aim of this work is to discuss the corrosion mechanism of Al alloys in anhydrous ethanol and to apply data-based statistical methods on experiments with AA1050 alloy in water-free ethanol in order to forecast time-dependent pitting susceptibility and pit sizes. The results will be the base in development of a comprehensive model which is able to simulate Al alloy corrosion behavior in ethanol containing fuels.

2 Preliminary consideratons

2.1 Competing pit growth reaction mechanisms

As mentioned in the introduction, the growth mechanism of Al alloy high temperature localized corrosion can not solely be viewed with the established electrochemical mechanistic assumptions which are known from room-temperature aqueous corrosion. Here, an attempt to understand the interplay between possible corrosion modes is made.

It is well accepted that "classical", aqueous pitting corrosion occurs due to a localized damage in the passive layer which is stimulated by aggressive anions. In the growth phase, the pit surface becomes anodic and the passive layer outside is cathodic. The process is accelerated by possible cathodic inclusions. The driving force of the dissolution is the potential gradient between the two short-circuited microelectrodes and their geometric relation.[20] That concept implies locally separated electrochemical reactions. However, there is evidence for the existence of a different mechanism. The potential-independent process can be regarded as "chemical corrosion" and was reported for numerous elements in aqueous solutions, including Fe,[14, 21] Ni[21, 22] and Al.[21, 23] The electron transfer takes place directly between a metal atom and the oxidant without inducing a current flow in the electrode.[24] There are several factors that make the aforementioned chemical corrosion mechanism predominant in the system under investigation:

- The analyzed pits on the surfaces exhibit remarkably uniform shapes (see sec. 4.1). Geometrical effects of potential driven corrosion reactions would induce some kind of asymmetry, depending on the relative position of the microelectrodes and the induced electric field.

- The initial conductivity of the utilized ethanol was measured at around $0.1\,\mu S\,cm^{-1}$. The low value is caused by the absence of ions and a low autoprotolysis constant of EtOH which makes a rapid electrochemical reaction unlikely.

- Due to the different apparent activation energies and thus, temperature dependencies of the chemical and electrochemical processes, it is expected that at high temperatures the chemical mechanism predominates.[25, 26] The assumption is supported by findings of Krüger *et al.* who measured up to three orders of magnitude larger mass losses gravimetrically compared to the calculated values from electrochemical current measurements. The deviations increased with higher temperatures.[7]

- Thomson *et al.* did not find any differences in corrosion kinetics despite galvanically coupling Al to brass, stainless steel or copper in practically water-free ethanol.[9]

We postulate that the molar Al dissolution flux across the active pit surface is a sum of a chemical and electrochemical reaction. The fractional contribution of each depends on the experimental variables. Assuming an adsorption-reaction mechanism for the chemical rate and an activation-controlled electrochemical process, it can be written:

$$j_{\mathrm{tot}} = j_{\mathrm{chem}} + j_{\mathrm{echem}} \tag{1}$$

$$j_{\mathrm{chem}} = \frac{k_{\mathrm{ads}} k_{\mathrm{r}} c(\mathrm{EtOH}) \Gamma}{k_{\mathrm{ads}} c(\mathrm{EtOH}) + k_{\mathrm{r}}} \tag{2}$$

$$j_{\mathrm{echem}} = \frac{i_{\mathrm{corr}}}{z\mathrm{F}} \left[\exp\left(\frac{2.3\eta}{\beta_{\mathrm{a}}} \right) - \exp\left(- \frac{2.3\eta}{\beta_{\mathrm{c}}} \right) \right] \tag{3}$$

where k_{ads} and k_{r} are the kinetic constants of adsorption and reaction, respectively, $c(\mathrm{EtOH})$ is the ethanol concentration, Γ the total surface site concentration. The electrochemical path is formulated in terms of the easily accessable corrosion current density i_{corr} and the anodic and cathodic Tafel parameters β_{a} and β_{c}. The chemical path is considered to be a consecutive adsorption of an ethanol molecule and a reaction to "Al-EtO" complex. The rates are characterized by respective kinetic constants. The units of the electrochemical reaction j_{echem} have to be adjusted to a molar flux in order to be summable to j_{chem}. The ethanol concentration dependence of j_{chem} is assumed to be of first order but might be different according to the exact mechanism. The parameters k_{ads} and k_{r} have an Arrhenius type temperature dependence but different apparent activation energies. The dependence of i_{corr} on temperature is more complex because two half-reactions with separate exchange current densities are involved.

Estimations of the temperature dependence of the electrochemical reaction can be made based on the measurements of Kramer *et al.*.[13] Corrosion current densities of AA1050 in anhydrous ethanol were approximated by means of Tafel analysis at different temperatures. It increased from $0.039\,\mu\mathrm{A\,cm^{-1}}$ at $25\,^{\circ}\mathrm{C}$ to only $0.069\,\mu\mathrm{A\,cm^{-1}}$ at $50\,^{\circ}\mathrm{C}$. The absolute values should be treated with care because the pitting mechanism was not taken into account. However, the marginal increase of 76 % can be considered as indication for weak temperature dependence.

In Fig. 1, a schematic Arrhenius plot of chemical and electrochemical reaction kinetics is shown. The larger activation energy of the chemical flux j_{chem} is, depending on the rate determining step, either adsorption or reaction related, leading to a stronger dependence on temperature. Thus, a positive correlation between temperature and j_{chem}. Because j_{chem} is only estimated, it can not be stated whether and where there exists an intersection point of j_{chem} and j_{echem}. Furthermore, it has to be noted that the use of the term "activation energy" only applies to elemental reaction steps and especially in case of the electrochemical reaction the term "apparent activation energy" is more appropriate. Nonetheless, the scheme is able to sketch the general competing mechanism.

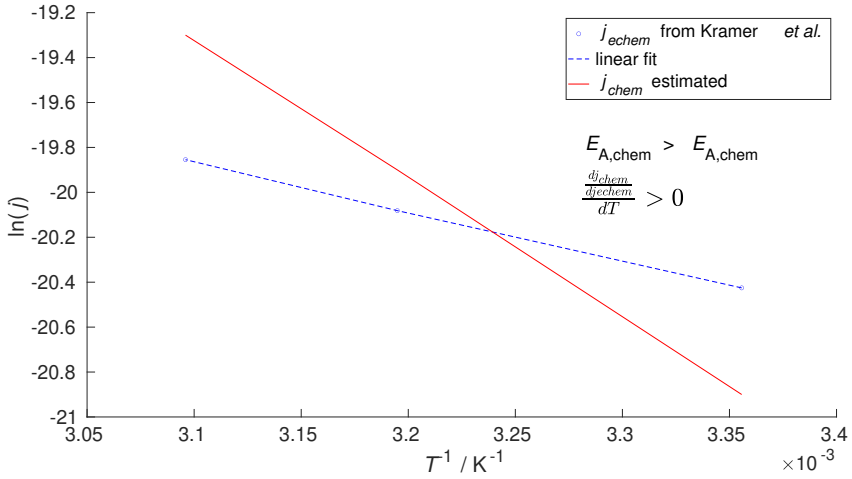

Figure 1: Effect of different apparent activation energies on chemical and electrochemical reaction kinetics. Data points for j_{echem} were taken from Ref. [13] for AA1050.

The fact that the Arrhenius plot of j_{echem} shows linear behavior for the measured temperatures (25-50 °C) enables the possibility of extrapolation for temperatures at which electrochemical measurements become inconvenient, assuming no limiting factors appear. The estimated parameters for j_{echem} are $E_{\mathrm{A}} = 18.2\,\mathrm{kJ\,mol^{-1}}$ and $A = 2.11 \times 10^{-6}\,\mathrm{mol\,m^{-2}\,s^{-1}}$.

The proposed simple model from eq. 1 can be expanded under consideration of intermediates as shown in Fig. 2. Anodic dissolution of Al under applied potential involves the electrochemical 1e-oxidation of Al atom to a surface-bound monovalent Al ion (step 1b).[15, 27, 28] Only from this intermediate, further 2e-oxidation leads to the formation of a trivalent cation. Step 2b is slow and therefore, rate-determining.[28] However, Al^+ can be complexated by an ethanol molecule in reaction 2a to form a surface complex. A direct chemical oxidation of an Al atom (1a) by an ethanol molecule is another possible pathway to the described complex. This is a Kolotyrkin-type "chemical" surface-reaction. Steps 1a and 2a are EtOH concentration-dependent reactions whereas 1b and 2b are typical electrochemical, potential-dependent processes. In step 3, the complex desorbs from the surface into bulk solution. The stability of such complexes was proven to be higher in non-aqueous alcoholic solvents.[27] A homogeneous red-ox-reaction (step 4) with two ethanol molecules leads to formation of molecular hydrogen and aluminium ethanolate. This pathway would explain the colloidal state of the corrosion product which is frequently observed.[8, 10, 12]

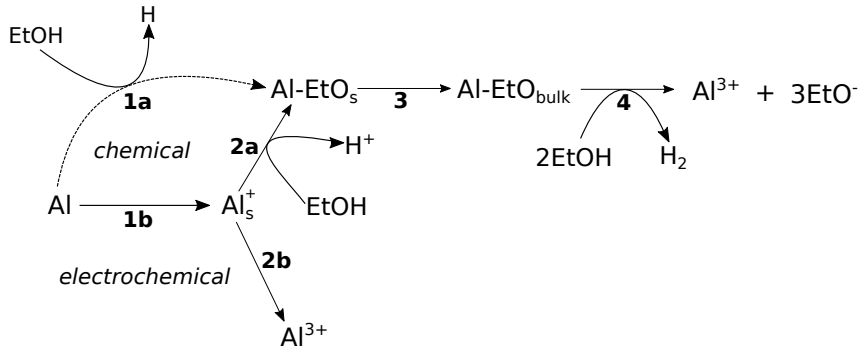

Figure 2: Possible scheme of competition between chemical and electrochemical mechanisms of Al dissolution in anhydrous ethanol. Index s stands for surface species.

With the currently employed apparatus, there is no possibility to directly distinguish between the pathways by means of a "post mortem" analysis. However, the estimated kinetic parameters based on generated data can be regarded as j_{tot} and the contributions of each flux can then be estimated based on electrochemical measurements from literature.

3 Experimental

Preparation of specimen: The experiments were conducted using commercially pure aluminium - Al EN AW 1050A procured from an industrial manufacturer having 99.5 % Al purity with the main impurity being Fe (0.32 %). Identical test samples (50 mm x 10 mm x 5 mm) were cut along the rolling direction, containing different grain structures on consequent faces as indicated by EBSD (Fig. 3). Only the 50 x 10 mm surfaced were considered for pit analysis in order to ensure a homogeneous surface for pit initiation. The samples were ground on all sides by means of a well lubricated silica wheel of grit P1000 at a considerably low speed, avoiding silica embedment on the surface.

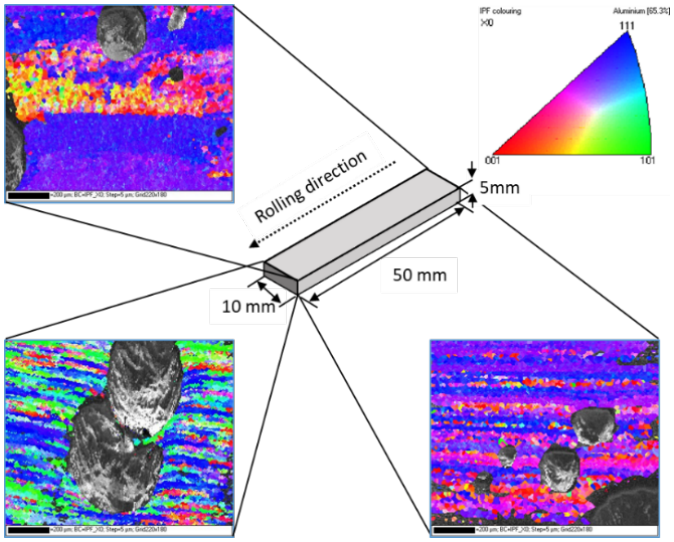

Figure 3: Sample dimensions with respective EBSD images after experiments indicating different grain structures depending on rolling direction.

Experiment description: High-pressure autoclaves/reactors were implemented to conduct the necessary experiments. As shown in Fig. 4, for each experiment, a freshly ground sample was placed in a reactor using PTFE holders. High purity anhydrous ethanol was used for the experiments (Carl Roth ROTIPURAN® $\geq$ 99.8 %) containing 0.03 $\pm$ 0.01 v/v % water, measured using Karl-Fischer titration. For each experiment, 200 mL ethanol was directly loaded using a tube, from the bottle to the closed reactor, through the pressure relief valve. As ethanol is known for its water affinity, this method established a uniform and low water contamination in every experiment. During the test, pressure and temperatures (reactor wall/medium) were periodically recorded every 15 seconds with an accuracy of 0.1 bar and 0.1 °C, respectively. After the experiments, samples were cleaned using concentrated nitric acid and photographed using optical microscopes. Pit analysis was conducted using ImageJ software.

Statistical analysis: Analysis of pit maxima was conducted according to block-maxima method.[18] The reacted sample was subdivided into ten equally sized coupons and the size of the largest pit was measured. These were regarded as independent and identically distributed (iid) random variables and thus, suitable for extreme-value analysis.

According to Fisher-Tippett-Gnedenko theorem, extreme value distributions converge to three asymptotic cases: Weibull, Gumbel and Frechet.[29, 30] All of them can be expressed in the Jenkinson-von-Mises parametrization depending on a shape parameter ξ:[31, 32]

$$\xi = 0 \qquad G(x;\mu,\beta) = \exp[-\exp(-\frac{x-\mu}{\beta})] \tag{4}$$

$$\xi \neq 0 \qquad G(x;\mu,\beta) = \exp(-[1+\xi(\frac{x-\mu}{\beta})]^{-1/\xi}) \tag{5}$$

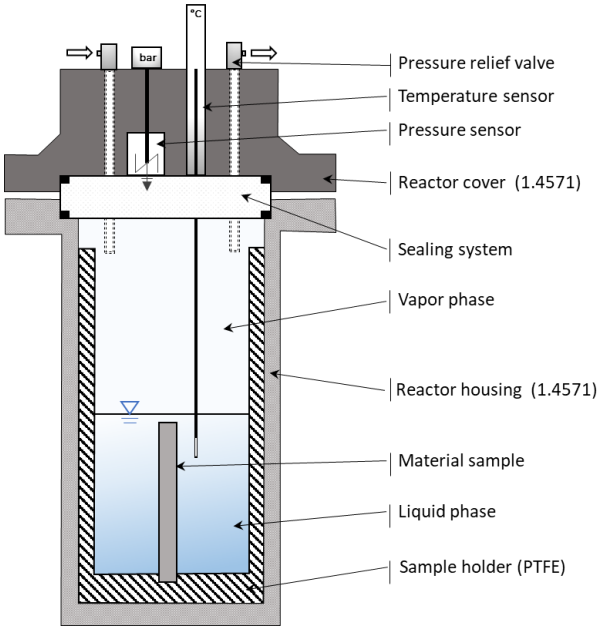

Figure 4: Schematic reactor setup for pit data generation.

where $\xi = 0$ corresponds to a Gumbel distribution with an exponential tail. The Frechet distribution has a positive ξ and a polynomial decay whereas the Weibull distribution corresponds to a negative ξ and a finite upper endpoint. The variables $\mu \in \mathbb{Z}$ and $\beta > 0$ are the location and shape parameters, respectively.

Probability weighted moments b_r of data samples X_i can be calculated :[33]

$$b_0 = n^{-1} \sum_{\mathrm{i}=1}^{n} X_\mathrm{i} \tag{6}$$

$$b_\mathrm{r} = n^{-1} \sum_{\mathrm{i}=1}^{n} \frac{(i-1)(i-2)\cdots(i-r)}{(n-1)(n-2)\cdots(n-r)} X_\mathrm{i} \tag{7}$$

The first two L-moments l are related to b:[34, 35]

$$l_1 = b_0 \tag{8}$$

$$l_2 = 2b_1 - b_0 \tag{9}$$

The Gumbel parameters can be expressed by means of L-moments:[34]

$$\mu = l_1 - \gamma\beta \tag{10}$$

$$\beta = \frac{l_2}{\log 2} \tag{11}$$

where γ is the Euler-Mascheroni constant.

The null-hypothesis that the iid samples are actually drawn from a Gumbel distribution was tested by means of the Modified Anderson-Darling (MAD) test for maxima. The test ensures that deviations of the tested distribution from a hypothetical distribution with known parameters are penalized to a higher degree on the upper end. The corresponding MAD test value AU^2_n for maxima is:[36]

$$AU_{\mathrm{n}}^2 = n \int_{-\infty}^{\infty} \frac{[G_{\mathrm{n}}(x) - G(x)]^2}{1 - G(x)} dG(x) \tag{12}$$

and the derived formula for computation is:[36]

$$AU_{\mathrm{n}}^2 = \frac{n}{2} - 2\sum_{\mathrm{i}=1}^{n} G(x_{\mathrm{i}}) - \sum_{\mathrm{i}=1}^{n} \left[2 - \frac{2i-1}{n}\right] \log(1 - G(x_{\mathrm{i}})) \tag{13}$$

where n is the number of extreme pit sizes, $G(x)$ is the cumulative distribution function and $G_{\mathrm{n}}(x)$ is the empirical distribution function with estimated parameters.

The AU_{n}^2 values are then used to estimate the corresponding p value in order to reject or accept the null hypothesis. In order to calculate a p-value for each assigned distribution function, a Monte Carlo procedure was employed. $N(MC) = 10000$ samples with n observations each were generated according to the estimated Gumbel parameters. For each of the samples, the MAD test was conducted. Thus, the percentage of smaller AU_{n}^2 values compared to the observed AU_{n}^2 value is related to the p-value:

$$p = 1 - \frac{N[AU_{\mathrm{n}}^2(\mathrm{calc}) < AU_{\mathrm{n}}^2(\mathrm{obs})]}{N(MC)} \tag{14}$$

With a commonly chosen significance level of 5 %, the hypotheses of all specimen with $p < 0.05$ are rejected and thus, are considered not in a Gumbel attraction domain.

At this point, it is emphasized that if a sufficient amount of data can be generated (e.g. for other alloys and liquid composition), a machine learning algorithm can easily be written based on the aforementioned equations in order to facilitate a faster forecast method.

4 Data analysis and discussion

4.1 Pre-processing of experimental data

Because the reaction has to be conducted in a closed, pressure-sealed vessel, it leads to some issues regarding the accessible data. The absence of an optical contact and the non-electrochemical nature of corrosion complicate tracking of pitting initiation and progress. A way to estimate reaction times based on accessible data is presented here. Only two parameters can be precisely measured with respective sensors: pressure and temperature. The measured pressure in the reaction vessel is a sum of the ethanol vapor pressure and hydrogen partial pressure:

$$p_{\text{vessel}} = p_{\text{EtOH}} + p_{\text{H}_2} \tag{15}$$

The empiric Antoine equation for the ethanol vapor pressure in the temperature range of interest is:[37]

$$p_{\text{EtOH,calc}} = 10^{4.9253 - \frac{1432.53}{-61.82+T}} \tag{16}$$

In addition, one has to account for the solubility of hydrogen in ethanol which delays the pressure rise by some time span. The molar fraction is given by:[38]

$$x_{\text{H2}} = 0.000016(p_{\text{H}_2} T) + 0.000594 \tag{17}$$

With the above considerations, it seems possible to approximate the onset of pitting because the overall reaction equation

$$\text{Al} + 3\,\text{C}_2\text{H}_5\text{OH} \longrightarrow \text{Al}^{3+} + 3\,\text{C}_2\text{H}_5\text{O}^- + \frac{3}{2}\,\text{H}_2 \tag{18}$$

implies that corrosion is accompanied by hydrogen evolution.

In Fig. 5 (a), a schematic reaction progress of a typical experiment is shown. The first stage t_{heat} represents the external heating of the reaction vessel to the preset temperature (red). The process induces a simultaneous ethanol vapor pressure rise (green). After the temperature is reached, the induction phase t_{ind} is characterized by a constant temperature and pressure. When the first pits start growing due to local breakdown of the passive layer in the reaction phase t_{r}, a pressure rise can be measured due to evolving hydrogen (yellow). Because the reaction is exothermic, the temperature slightly increases as well. The reaction is interrupted when a certain predefined pressure threshold is reached. Without a threshold, the reaction would proceed auto-catalytically and converts the specimen to corrosion product without the possibility of analyzing the pits.

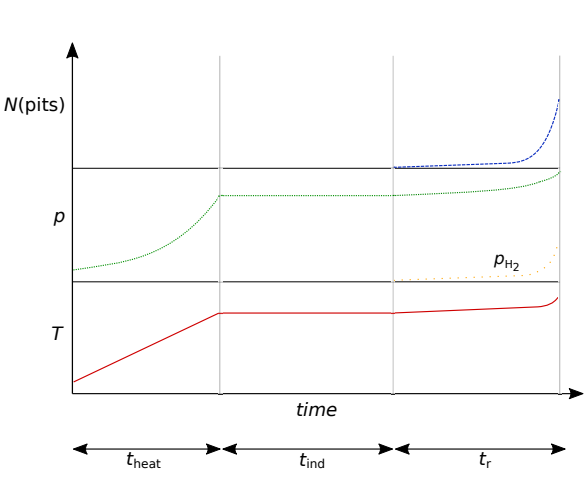

(a) Schematic diagram of T, p and number of pits with arbitrary units.

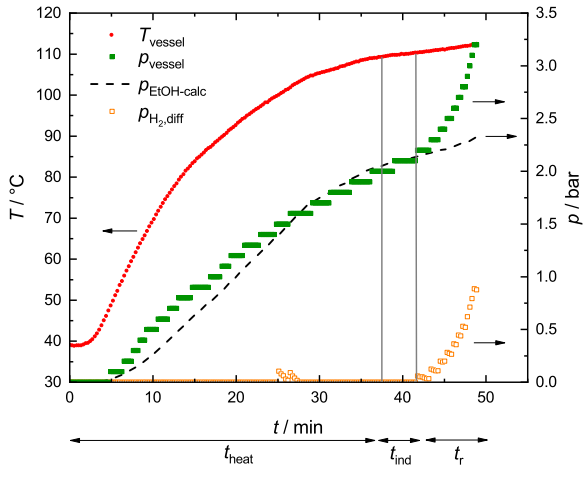

(b) Real measured T and p values with calculated vapor pressure of ethanol and resulting H_2 pressure.

Figure 5: Development of temperature and pressure in a typical experiment with corresponding specific time intervals.

In Fig. 5 (b), exemplary real temperature and pressure data is shown. The ethanol vapor pressure was calculated according to eq. 16 and 17. Measurable pitting starts at around 42 minutes after a heating time of 37 minutes and an induction time of approximately five minutes. The data resembles the theoretical curves from (a) by and large. The small pressure rise at 26 minutes and 100 °C can be attributed to evaporation of physisorbed water in the vessel.

Of course, the strict time subdivisions in Fig. 5 (a) and (b) are very idealized. The line between t_{ind} and t_{r} is probably not that strict. In fact, because the employed reactor is not able to detect small pressure jumps (accuracy 0.1 bar), formation of the very first pits can not be measured precisely. This might lead to problems in the extreme value analysis, as will be shown in section 4.3. In addition, the energy release of the corrosion reaction leads to a simultaneous temperature rise in the vessel, which probably has a significant effect on the initiation process. This is a big disadvantage in contrast to electrochemical pitting corrosion experiments where a potential can be exactly set for the whole experiment and the starting point is precise.

A total pit size distribution histogram of sample with $t_{\mathrm{R}} = 344\,\mathrm{s}$ and $T = 110\,^{\circ}\mathrm{C}$ is exemplary shown in Fig. 6. The distribution seems unimodal which corresponds to only one population of pits which supports the assumption of non-existent metastability. As can be seen in the inset, the pit population is randomly distributed over the sample surface. As can be seen from the fitting curves, lognormal distribution is more appropriate for the pit population than Gauss distribution. The same tendency was observed for all analyzed samples and confirmed by maximum likelihood calculations. Lognormal distributions are commonly found as a realization of multiplicative, non-linear, random processes.[39] In this case, the finding can be interpreted in terms of the pit initiation process: The locally different, temperature-dependent dehydration probabilities are multiplied for probability calculation of a critical state at which a pit nucleates. The resulting nucleation times and thus, the pit sizes, then converge to a lognormal distribution.

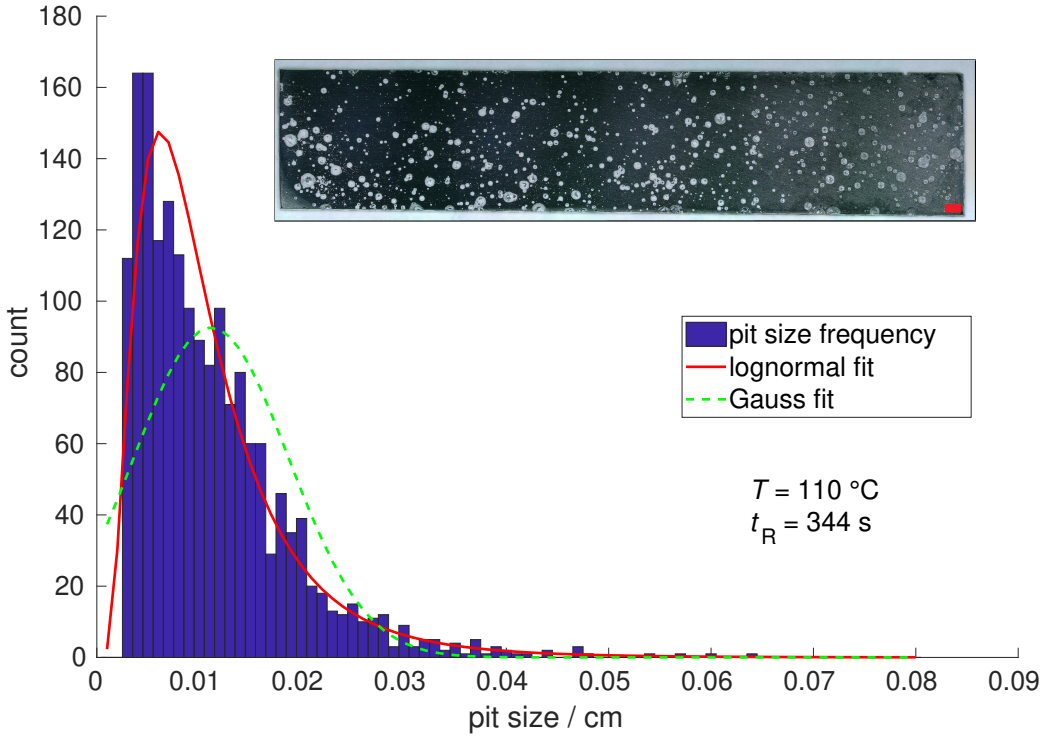

Figure 6: Exemplary histogram of pit size distribution of a reacted AA1050 specimen with corresponding Gauss (dashed) and lognormal (solid) distribution fit. The reaction temperature was set to 110 °C and t_{R} was 344 s. The analysed area was 2.5 cm^2. The inset shows a micrograph of the specimen after reaction (scale bar = 0.1 cm).

In Fig. 7, an exemplary micrograph and a depth profile of the largest pit after reaction at 110 °C is shown. At the bottom, a perforation was caused by a pit originating at the opposite site of the speecimen. The

apparent hexagonal shape is remarkable and not typical of regular aqueous corrosion experiments. In fact, all of the observed pits exhibit a very similar shape. The shapes might be formed due to direction dependent chemical dissolution kinetics as known from e.g. anisotropic etching.[40] However, the shape is a bit puzzling because Al crystallizes in a face-centered cubic structure and thus, does not exhibit a trigonal symmetry. There might be a connection to the hexagonal corundum (α-Al_2O_3) structure but this aspect requires further study. Nonetheless, we believe that the symmetric appearance and lack of secondary pits is a strong indicator for a predominantly chemical corrosion mechanism.

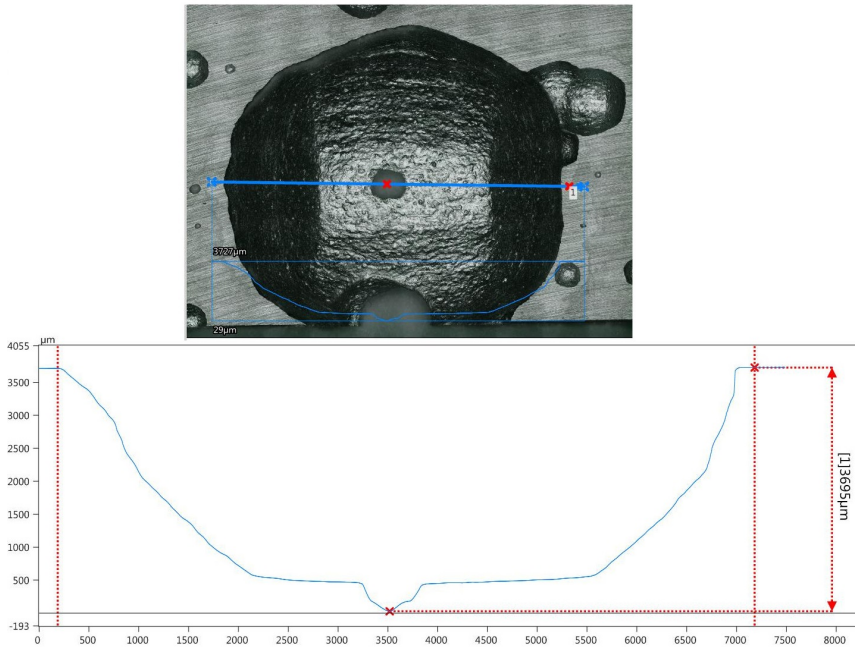

Figure 7: Micropgraph and depth profile of the largest pit on AA1050 specimen after reaction at 110 °C.

4.2 Induction times analysis

The uncertainty of experimental outcomes and high data scattering is well known for alcoholate corrosion of Al alloys.[8, 9] In this section, it is assessed whether a statistical analysis can be employed for the description of the highly stochastic nature of passive layer breakdown events which can facilitate a non-trivial comparison between experiments. Weibull distribution is often employed for dealing with pitting related problems.[19, 41, 42] Here, we fit the measured induction times t_{ind} to the function in order to calculate a robust expected value of corrosion onset. The density function of the Weibull distribution is

$$f(t;\lambda,k) = \frac{k}{\lambda}(t/\lambda)^{k-1}\exp(-(t/\lambda)^k) \tag{19}$$

and the cumulative distribution is

$$F(t;\lambda,k) = 1 - \exp(-(t/\lambda)^k) \tag{20}$$

where $k > 0$ is the shape parameter and $\lambda > 0$ is the scale parameter.

In order to obtain the Weibull parameters it is necessary to plot $\ln(t_{\mathrm{ind}})$ vs $\ln(\ln[\frac{1}{1-F(t_{\mathrm{ind}})}])$. The cumulative distribution F is calculated as follows: The induction times are sorted in ascending order as seen in Tab. 1. For each t_{ind} with an assigned order i, $F(t_{\mathrm{ind}}) = \frac{i}{N+1}$ where N is the total number of experiments (here 8). Linear fitting of the data for $T = 105\,^{\circ}\mathrm{C}$ and $110\,^{\circ}\mathrm{C}$ is shown in Fig. 8 (a). The resulting parameters and expected values are summarized in Tab. 2 It can be stated that the induction times can be fitted sufficiently well to the Weibull distribution. As expected, the mean increases with higher temperature. It is notable that both shape parameters k are close to or equal unity which corresponds to an exponential distribution. A steeper rise of the cumulative probability of $t_{\mathrm{ind}}(110\,^{\circ}\mathrm{C})$ compared to $t_{\mathrm{ind}}(105\,^{\circ}\mathrm{C})$ can be seen in Fig. 8 (b) which represents a higher failure probability at shorter times.

Table 1: Summary of induction times t_{ind} in ascending order for experiments at 105 °C and 110 °C, respectively.

i	$T = 105\,^{\circ}\mathrm{C}$ / s	$T = 110\,^{\circ}\mathrm{C}$ / s
1	120	49
2	438	75
3	660	163
4	774	165
5	786	181
6	924	346
7	1770	491
8	3438	840

The question whether a clear physical meaning can be assigned to the calculated parameters can be answered considering the assumed pit initiation mechanism. If dehydration of gibbsite to boehemite and alumina and the accompanying formation of pores in the passive layer is the critical factor, the temperature has a crucial effect on the reaction kinetics as was shown in several publications.[43, 44] Thus, it is feasible to assume that λ is proportional to the kinetic constant of the dehydration process but also to the composition and structure of the passive layer which defines the local critical water loss for pit formation. Because those parameters are difficult to access experimentally, λ might be used as a characteristic failure probability estimator for an alloy and temperature combination.

The applied statistical analysis certainly enables a more quantitative prediction of component integrity of AA1050 due to dry corrosion. However, caution is advised due to the presumptions that were made. It can not be excluded that first pits initiate prior to the measurable reaction time onset. For a more profound failure probability analysis it would be advantageous to facilitate detection of the very first pits.

Table 2: Estimated Weibull scale and shape parameters for measurable pitting induction times at different temperatures and deduced expected mean values.

T / °C	k	λ / s	mean / s	R^2
105	0.947	7.83×10^{-4}	1240	0.926
110	1.00	3.03×10^{-3}	330	0.953

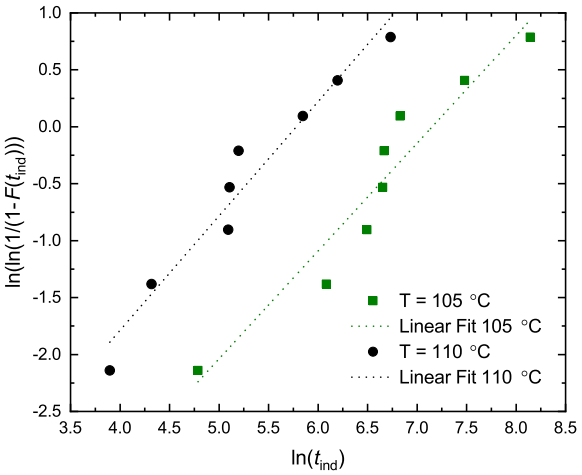

(a) Linear fit of pitting induction times on AA1050 at 105 °C and 110 °C in a Weibull plot.

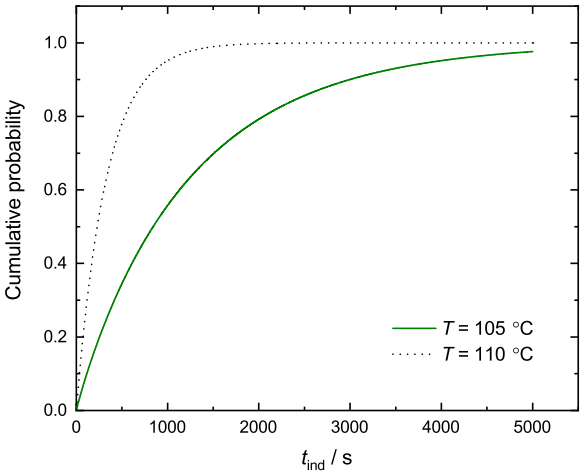

(b) Cumulative probability functions of the pitting induction times on AA1050 at 105 °C and 110 °C.

Figure 8: Statistical analysis of pitting induction times on AA1050 in anhydrous ethanol.

4.3 Pit Extreme Value Analysis

It is well accepted that pits initiate at defective sites of the passive layer and the process is stimulated by aggressive anions.[45] However, in our case, it is assumed that the passive layer is disrupted by temperature-induced water loss of aluminium hydroxide and boehemite.[12] Here, we aim to elaborate whether the extreme value theorem can be applied to generated experimental data in order to predict maximum pit sizes on Al alloys.

In order to be able to apply the extreme value analysis to any problems, the drawn values have to be identically independently distributed (iid).[46] This presumption was doubted by Melchers who emphasized the effect of metastable growth on the final pit population.[16] However, a requirement for metastability is the possibility of repassivation which is not met in water-free environment. The lack of passive layer and the present potential-independent, chemical corrosion ensures that existing pits continuously propagate.

The successful application of the procedure also implies an unchanging growth law for entire observation time.[16, 47] It might be problematic for very long exposure times and varying growth functions, however, in our research the experiment times are fairly short in comparison to typical corrosion experiments.

The Gumbel parameters β and μ can be estimated by plotting the block maxima appropriately against the empirical cumulative distribution and performing a regression analysis.[19, 41, 48, 49] These so called Gumbel probability papers use a double-logarithmic form of eq. 4 where the empirical cumulative probability G is calculated analogous to the procedure described in section 4.2.[17, 18, 48, 50, 51] For the sake of visualization, classical Gumbel plots are shown in Fig. 9 and 10. The curves show good linearity for most of the samples which indicates right choice of parent distribution function.

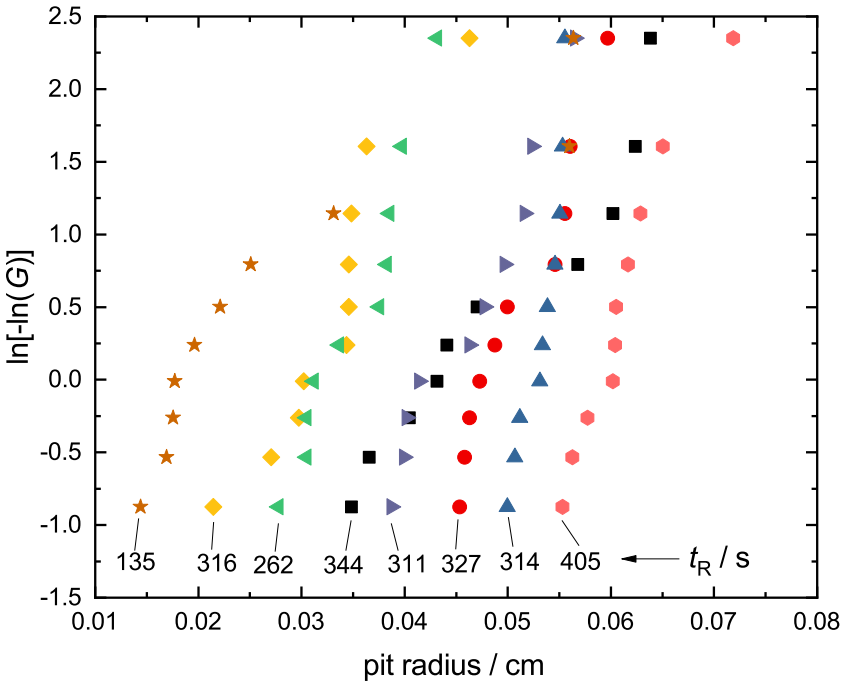

Figure 9: Gumbel plots of pit block maxima radii from reacted AA1050 specimen at 110 °C with corresponding reaction times t_R. All samples fall into Gumbel domain of attraction.

However, there are more reliable methods for Gumbel parameter estimations. These include techniques like maximum likelihood method[52–54], method of moments and method of probability weighted moments.[34, 55] There is strong evidence that the method of probability weighted moments outperforms the

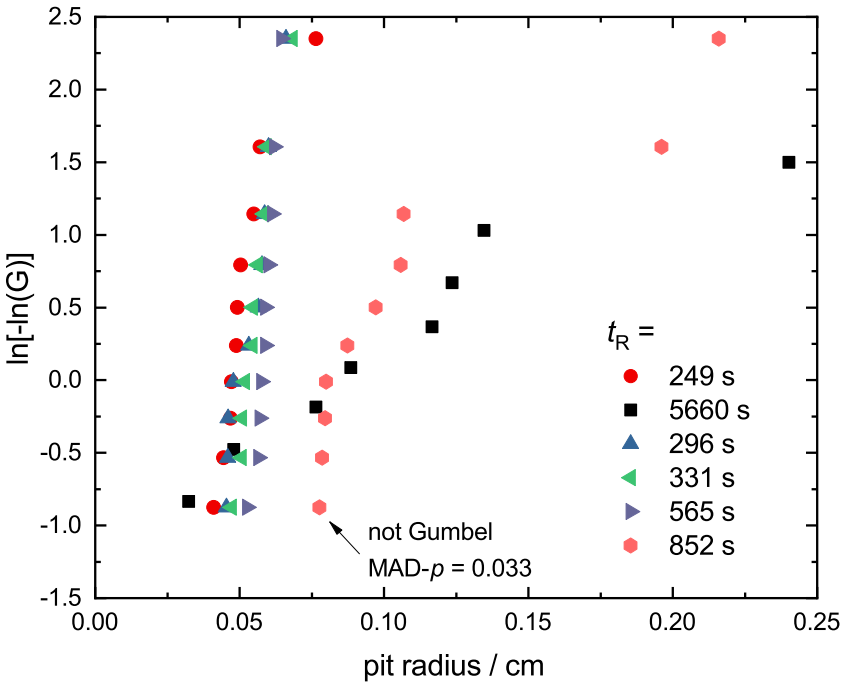

Figure 10: Gumbel plots of pit block maxima radii from reacted AA1050 specimen at 105 °C with corresponding reaction times t_R. Sample with $t_R = 852$ s is rejected by MAD test and is thus not in Gumbel domain of attraction.

other procedures, especially for small sample sizes.[56, 57] Thus, probability of weighted moments (PWM) method was used as unbiased estimator by means of L-moments calculation introduced by Hosking.[35]

The calculated Gumbel parameters are summarized in Tab. 3 for $T = 110$ °C and in Tab. 4 for $T = 105$ °C. For quantitative assessment of the fit, the obtained Gumbel parameters were tested by means of the modified Anderson-Darling (MAD) goodness-of-fit test for Gumbel distributions.[36, 58] It was proven to be superior to other significance tests like chi-square, Kolmogorov-Smirnov or Cramer-von-Mises, especially for low sample sizes.[59] The p-value was used as the null-hypothesis rejection criterion. For a significance level $\alpha = 0.05$, the null hypothesis could not be rejected for almost all analyzed samples. Only sample No. 14 exhibits a lower p-value and thus, the sizes can not be described by Gumbel distribution. This is supported by the curve in Fig. 10 where the slope deviates strongly from a linear trend. Attempts to fit the data to other extreme value distributions were unsuccessful. The reason could be slight inconsistencies in surface treatment (especially Si inclusions at the sample edges due to polishing procedure) and the resulting varying pitting susceptibility and corresponding violation of the iid criterion. Preliminary test revealed strong pitting sensitivity to surface preparation of the specimen. Nonetheless, because the issue only appeared on one of 14 specimen, it can be stated that Gumbel analysis is an appropriate distribution for extreme pit sizes on AA1050 in pure ethanol.

As the next step, the Gumbel parameters were correlated to the reaction time t_R which is shown in Fig. 11. It can be seen from Fig. 11 (a) and (b) that for the higher reaction temperature, both β and μ have a positive correlation. This behavior is expected and was frequently reported for potential-driven aqueous pitting experiments.[17, 51] For the lower reaction temperature, the correlation is less clear. It looks inversely proportional for β at low t_R but increases for the longest reacting specimen. A positive correlation of μ at low t_R can be seen in Fig. 11 (b) but the trend is disrupted by the longest reacting specimen.

In Fig. 12, a plot of expected maximum pit radii against the reaction time is shown. The expected values were calculated by means of the Gumbel parameters according to the equation

$$E(X) = \mu + \beta\gamma \tag{21}$$

Table 3: PWM estimated Gumbel parameters and corresponding modified Anderson-Darling (MAD) p-values of specimen which reacted at 110 °C for different duration. β and μ can be interpreted as standard deviation and mean of maximum pit radii whereas the p-value is a measure for the correctness of the chosen parent distribution.

Sample No.	t_R / s	$\beta \cdot 10^{-3}$ / cm	$\mu \cdot 10^{-3}$ / cm	MAD p-value
1	344	21.5	36.4	0.616
2	327	9.97	45.2	0.810
3	314	3.99	51.0	0.095
4	316	12.0	26.0	0.074
5	262	9.97	29.4	0.441
6	311	12.3	39.4	0.662
7	135	2.79	11.8	0.228
8	405	8.97	61.2	0.499

Table 4: PWM estimated Gumbel parameters and corresponding modified Anderson-Darling (MAD) p-values of specimen which reacted at 105 °C for different duration. β and μ can be interpreted as standard deviation and mean of maximum pit radii whereas the p-value is a measure for the correctness of the chosen parent distribution.

Sample No.	t_R / s	$\beta \cdot 10^{-3}$ / cm	$\mu \cdot 10^{-3}$ / cm	MAD p-value
9	249	16.9	41.8	0.357
10	5660	172	31.4	0.668
11	296	13.9	45.6	0.226
12	331	11.3	48.6	0.943
13	565	6.30	55.3	0.837
14	852	84.3	63.7	**0.033**

The use of those values instead of true maximum pit sizes takes into account the stochastic nature of the pit initiation times. R^2 values of the linear fitting functions suggest very good correlation for the lower temperature and a moderate correlation for the higher temperature. As expected, the steeper slope corresponds to the higher temperature. It has to be noted that the results do not necessarily imply a linear growth law. The fitting should be viewed as a confirmation of a positive correlation and emphasize the possibility estimating the pit sizes by means of data analysis. However, a deduction of a time dependent growth law is not yet exactly possible and requires a more precise apparatus.

Some reasons can be named for the observed discrepancies in the correlations:

- The fact that $T = 105\,°C$ is probably very close to the critical temperature where no pits are induced, might be problematic because the system is very sensitive to slight temperature fluctuations at this point.

- Because only extreme pit sizes are considered in Gumbel analysis, the probability is very high that those pits initiated before a measurable, hydrogen-induced pressure rise is detected. This implies an uncertainty between the measured and real t_R. Due to the fairly short overall reaction times, already small deviations can disturb correlations.

- We defined the end of reaction as the time when the pressure is released from the vessel. However, because the temperature is still high inside, the reaction is not interrupted immediately which leads to another inaccuracy in generated data.

Nonetheless, even with those uncertainty sources, the calculated kinetic parameters (i.e. the fitting slopes in Fig. 12) for respective temperatures can be compared with the extrapolated electrochemical fluxes based on results of Kramer *et al.*.[13] For 105 °C, $j_{\mathrm{tot},105\,°C} = 1.48 \times 10^{-2}\,\mathrm{mol\,m^{-2}\,s^{-1}}$ and $j_{\mathrm{echem},105\,°C} = 6.44 \times 10^{-9}\,\mathrm{mol\,m^{-2}\,s^{-1}}$ and for 110 °C $j_{\mathrm{tot},110\,°C} = 1.89 \times 10^{-1}\,\mathrm{mol\,m^{-2}\,s^{-1}}$ and $j_{\mathrm{echem},110\,°C} = 6.95 \times 10^{-9}\,\mathrm{mol\,m^{-2}\,s^{-1}}$. The values imply that the chemical fluxes are around seven orders of magni-

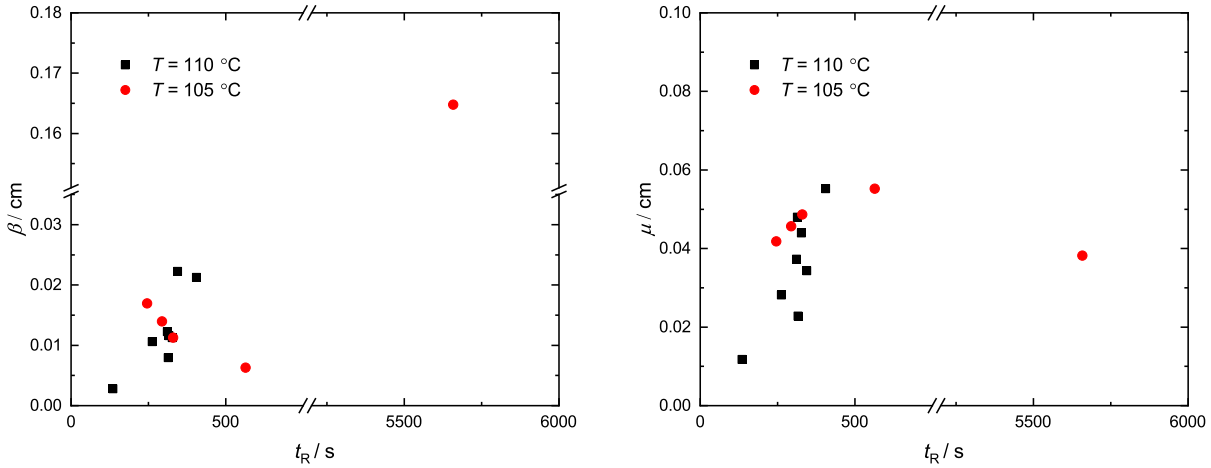

(a) Correlation of reaction time t_R to shape parameter β.

(b) Correlation of reaction time t_R to location parameter μ

Figure 11: Analysis of obtained Gumbel parameters at different reaction temperatures.

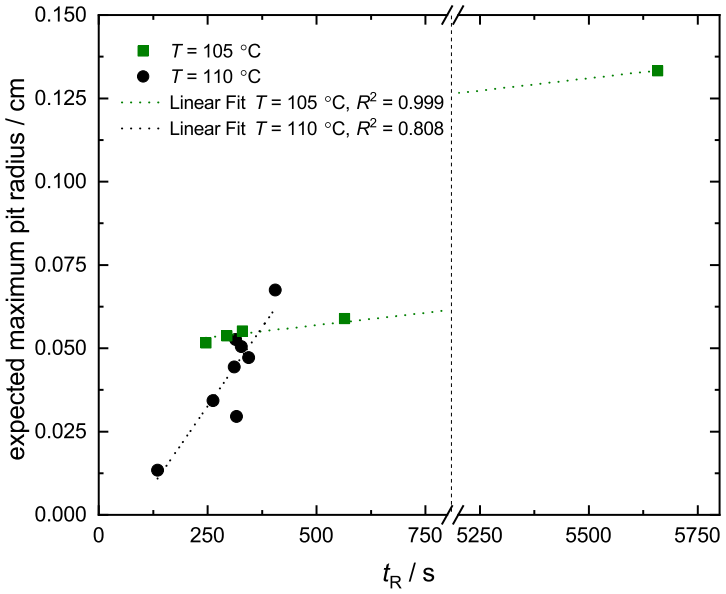

Figure 12: Plot and linear fit of expected pit radii against the reaction time t_R.

tude larger than the electrochemical fluxes at the examined temperatures. Furthermore, the proportion of j_chem to j_tot is one order of magnitude higher for 110 °C compared to 105 °C which supports the assumption of a significantly higher activation energy for the chemical process.

Although a time correlation to the calculated expected pit sizes is possible with the currently employed experimental procedures, one should question whether Gumbel analysis alone is sufficient for forecasting material resilience in the given environment. It is important to note that component failure can occur not only by perforation by a single pit but also due to a sudden temperature rise and accompanying autocatalytic increase of reaction kinetics and a switch to uniform corrosion. This was observed in several experiments when the reaction was not stopped and cooled in time. If the mechanism changes in that extreme way, predictions based on Gumbel analysis lose their validity. The exact reason fo the sudden mechanism change will be subject of a future study.

5 Conclusion

In this work, a data based approach for analysis of localized corrosion of aluminium alloys in water-free ethanol is presented on the example of AA1050. A possible reaction mechanism for dry alcoholate corrosion of Al is proposed and reasons for a predominantly chemical driving force are emphasized. On the example of AA1050, it is suggested to describe statistical uncertainties of the experiments by means of Weibull analysis of induction times. It allows a rough approximation of component failure times without having to determine the parameters which are related to pit-initiation process and hardly accessible experimentally.

Extreme value Gumbel analysis was employed for pit maxima characterization and it was shown that it is an appropriate model for the temperature-driven ethanolate corrosion by means of modified Anderson-Darling test and corresponding p-values. A positive correlation was shown for expected maximum pit sizes and the contribution of a chemical process was highlighted with regard to a necessity of employment of non-electrochemical methods.

It is expected to obtain more precise results with a smaller reactor in order to estimate the growth law equations and verify the proposed reaction mechanism.

Acknowledgments: The authors acknowledge the financial support by the Deutsche Forschungsgemeinschaft (DFG).

Literature

[1] S. Kent Hoekman. "Biofuels in the U.S. – Challenges and Opportunities". In: *Renewable Energy* 34.1 (Jan. 2009), pp. 14–22. DOI: 10.1016/j.renene.2008.04.030. URL: https://doi.org/10.1016/j.renene.2008.04.030.

[2] Katarzyna Robak and Maria Balcerek. "Review of Second-Generation Bioethanol Production from Residual Biomass". In: *Food Technology and Biotechnology* 56.2 (2018). DOI: 10.17113/ftb.56.02.18.5428. URL: https://doi.org/10.17113/ftb.56.02.18.5428.

[3] Jason Hill et al. "Environmental, economic, and energetic costs and benefits of biodiesel and ethanol biofuels". In: *Proceedings of the National Academy of sciences* 103.30 (2006), pp. 11206–11210.

[4] Osami Seri and Yasuhiro Kido. "Corrosion Phenomenon and Its Analysis of 6063 Aluminum Alloy in Ethyl Alcohol". In: *MATERIALS TRANSACTIONS* 50.6 (2009), pp. 1433–1439. DOI: 10.2320/matertrans.l-m2009806. URL: https://doi.org/10.2320/matertrans.l-m2009806.

[5] Y.H. Yoo et al. "Corrosion characteristics of aluminum alloy in bio-ethanol blended gasoline fuel: Part 1. The corrosion properties of aluminum alloy in high temperature fuels". In: *Fuel* 90.3 (Mar. 2011), pp. 1208–1214. DOI: 10.1016/j.fuel.2010.10.058. URL: https://doi.org/10.1016/j.fuel.2010.10.058.

[6] I.J. Park et al. "Corrosion characteristics of aluminum alloy in bio-ethanol blended gasoline fuel: Part 2. The effects of dissolved oxygen in the fuel". In: *Fuel* 90.2 (Feb. 2011), pp. 633–639. DOI: 10.1016/j.fuel.2010.09.049. URL: https://doi.org/10.1016/j.fuel.2010.09.049.

[7] L Krüger et al. "Corrosion behaviour of aluminium alloys in ethanol fuels". In: *Journal of Materials Science* 47.6 (2012), pp. 2798–2806.

[8] F Tuchscheerer et al. "Alkoholatkorrosion von Aluminium (EN AC-48100), Einfluss von Temperatur sowie Ethanol-und Wassergehalt". In: *Materialwissenschaft und Werkstofftechnik* 6.44 (2013), pp. 555–561.

[9] Jeffery K Thomson, Steven J Pawel, and Dane F Wilson. "Susceptibility of aluminum alloys to corrosion in simulated fuel blends containing ethanol". In: *Fuel* 111 (2013), pp. 592–597.

[10] In-Jun Park et al. "Evaluation of corrosion characteristics of aluminum alloys in the bio-ethanol gasoline blended fuel by 2-electrode electrochemical impedance spectroscopy". In: *Fuel* 126 (June 2014), pp. 26–31. DOI: 10.1016/j.fuel.2014.02.030. URL: https://doi.org/10.1016/j.fuel.2014.02.030.

[11] Edoardo Proverbio et al. "Susceptibility to corrosion of aluminium alloy components in ethanol adsorption chiller". In: *Renewable Energy* 110 (2017), pp. 174–179.

[12] Luigi Calabrese, Paolo Bruzzaniti, and Edoardo Proverbio. "Pitting corrosion of aluminum alloys in anhydrous ethanol". In: *Materials and Corrosion* 69.12 (July 2018), pp. 1815–1826. DOI: 10.1002/maco.201810125. URL: https://doi.org/10.1002/maco.201810125.

[13] Gustavo Raúl Kramer, Claudia Marcela Méndez, and Alicia Esther Ares. "Evaluation of Corrosion Resistance of Commercial Aluminum Alloys in Ethanol Solutions". In: *Materials Research* 21.6 (Oct. 2018). DOI: 10.1590/1980-5373-mr-2017-0272. URL: https://doi.org/10.1590/1980-5373-mr-2017-0272.

[14] Ya M Kolotyrkin and GM Florianovich. "Dissolution of iron, chromium, and their alloys in sulfuric acid by a chemical mechanism". In: *Zashch. Met* 1 (1965), pp. 7–12.

[15] M. Garreau and P. L. Bonora. "On the role of the anions on the anomalous anodic dissolution of aluminium". In: *Journal of Applied Electrochemistry* 7.3 (May 1977), pp. 197–209. DOI: 10.1007/bf00618986. URL: https://doi.org/10.1007/bf00618986.

[16] R. E. Melchers. "Statistical Characterization of Pitting Corrosion Part 1: Data Analysis". In: *CORROSION* 61.7 (July 2005), pp. 655–664. DOI: 10.5006/1.3278201. URL: https://doi.org/10.5006/1.3278201.

[17] A. Valor et al. "Stochastic modeling of pitting corrosion: A new model for initiation and growth of multiple corrosion pits". In: *Corrosion Science* 49.2 (Feb. 2007), pp. 559–579. DOI: 10.1016/j.corsci.2006.05.049. URL: https://doi.org/10.1016/j.corsci.2006.05.049.

[18] A. Valor et al. "Stochastic approach to pitting-corrosion-extreme modelling in low-carbon steel". In: *Corrosion Science* 52.3 (Mar. 2010), pp. 910–915. DOI: 10.1016/j.corsci.2009.11.011. URL: https://doi.org/10.1016/j.corsci.2009.11.011.

[19] Xuanpeng Li et al. “Modeling of Pitting Corrosion Damage Based on Electrochemical and Statistical Methods”. In: *Journal of The Electrochemical Society* 166.15 (2019), pp. C539–C549. DOI: 10.1149/2.0401915jes. URL: https://doi.org/10.1149/2.0401915jes.

[20] Z Szklarska-Smialowska and ZS-Smialowska. *Pitting and crevice corrosion*. Nace international Houston, TX, 2005.

[21] E Heitz and CM v. Meysenbug. “Die Korrosion von Eisen, Nickel, Kupfer und Aluminium in organischen Lösungsmitteln mit geringem Mineralsäuregehalt”. In: *Materials and Corrosion* 16.7 (1965), pp. 578–595.

[22] GG Penov et al. “MECHANISM UNDERLYING THE DISSOLUTION OF IRON, STEEL 20, AND NICKEL IN ACID SOLUTIONS”. In: *Zashchita Metallov* 6.5 (1970), pp. 544–547.

[23] DM Dražić and JP Popić. “Corrosion rates and negative difference effects for Al and some Al alloys”. In: *Journal of applied electrochemistry* 29.1 (1999), pp. 43–50.

[24] GM Florianovich. “Electroless dissolution of metals: substantiation and alternative notions”. In: *Russian Journal of Electrochemistry* 36.10 (2000), pp. 1037–1042.

[25] Jovan P Popić and Dragutin M Dražić. “Electrochemistry of active chromium, part III: Effects of temperature”. In: *Journal of the Serbian Chemical Society* 68.11 (2003), pp. 871–882.

[26] Dragutin M Dražić and Jovan P Popić. “Anomalous dissolution of metals and chemical corrosion”. In: *Journal of the Serbian Chemical Society* 70.3 (2005), pp. 489–511.

[27] J. Banas et al. “Corrosion and passivity of metals in methanol solutions of electrolytes”. In: *Journal of Solid State Electrochemistry* 13.11 (Sept. 2008), pp. 1669–1679. DOI: 10.1007/s10008-008-0649-5. URL: https://doi.org/10.1007/s10008-008-0649-5.

[28] Maria Starowicz, Pawel Starowicz, and Barbara Stypula. “Alumina-based nanoparticles obtained by anodic dissolution of Al in electrolytes with alcohol solvents”. In: *Journal of Solid State Electrochemistry* 18.11 (Mar. 2014), pp. 3065–3071. DOI: 10.1007/s10008-014-2447-6. URL: https://doi.org/10.1007/s10008-014-2447-6.

[29] Ronald Aylmer Fisher and Leonard Henry Caleb Tippett. “Limiting forms of the frequency distribution of the largest or smallest member of a sample”. In: *Mathematical Proceedings of the Cambridge Philosophical Society*. Vol. 24. 2. Cambridge University Press. 1928, pp. 180–190.

[30] B. Gnedenko. “Sur La Distribution Limite Du Terme Maximum D’Une Serie Aleatoire”. In: *Annals of Mathematics* 44.3 (1943), pp. 423–453. ISSN: 0003486X. URL: http://www.jstor.org/stable/1968974.

[31] Richard Von Mises. “La distribution de la plus grande de n valuers”. In: *Rev. math. Union interbalcanique* 1 (1936), pp. 141–160.

[32] Arthur F Jenkinson. “The frequency distribution of the annual maximum (or minimum) values of meteorological elements”. In: *Quarterly Journal of the Royal Meteorological Society* 81.348 (1955), pp. 158–171.

[33] J. Arthur Greenwood et al. “Probability weighted moments: Definition and relation to parameters of several distributions expressable in inverse form”. In: *Water Resources Research* 15.5 (Oct. 1979), pp. 1049–1054. DOI: 10.1029/wr015i005p01049. URL: https://doi.org/10.1029/wr015i005p01049.

[34] Jonathan Richard Morley Hosking, James R Wallis, and Eric F Wood. “Estimation of the generalized extreme-value distribution by the method of probability-weighted moments”. In: *Technometrics* 27.3 (1985), pp. 251–261.

[35] Jonathan RM Hosking. “L-moments: Analysis and estimation of distributions using linear combinations of order statistics”. In: *Journal of the Royal Statistical Society: Series B (Methodological)* 52.1 (1990), pp. 105–124.

[36] M. I. Ahmad, C. D. Sinclair, and B. D. Spurr. “Assessment of flood frequency models using empirical distribution function statistics”. In: *Water Resources Research* 24.8 (Aug. 1988), pp. 1323–1328. DOI: 10.1029/wr024i008p01323. URL: https://doi.org/10.1029/wr024i008p01323.

[37] D Ambrose, C.H.S Sprake, and R Townsend. “Thermodynamic properties of organic oxygen compounds XXXVII. Vapour pressures of methanol, ethanol, pentan-1-ol, and octan-1-ol from the normal boiling temperature to the critical temperature”. In: *The Journal of Chemical Thermodynamics* 7.2 (Feb. 1975), pp. 185–190. DOI: 10.1016/0021-9614(75)90267-0. URL: https://doi.org/10.1016/0021-9614(75)90267-0.

[38] Mani Safamirzaei, Hamid Modarress, and Mohsen Mohsen-Nia. "Modeling the hydrogen solubility in methanol, ethanol, 1-propanol and 1-butanol". In: *Fluid Phase Equilibria* 289.1 (Feb. 2010), pp. 32–39. DOI: 10.1016/j.fluid.2009.10.012. URL: https://doi.org/10.1016/j.fluid.2009.10.012.

[39] M. Kendall and A. Stuart. *The Advanced Theory of Statistics*. Vol. 1. Griffin, London, 1977.

[40] Osamu Tabata et al. "Anisotropic etching of silicon in TMAH solutions". In: *Sensors and Actuators A: Physical* 34.1 (1992), pp. 51–57.

[41] Su-Il Pyun, Eung-Jo Lee, and Gil-Soo Han. "Localized corrosion of sputtered Al-1wt.%Si-0.5wt.%Cu alloy thin film". In: *Thin Solid Films* 239.1 (Feb. 1994), pp. 74–78. DOI: 10.1016/0040-6090(94)90110-4. URL: https://doi.org/10.1016/0040-6090(94)90110-4.

[42] Tao Zhang et al. "Electrochemical noise analysis on the pit corrosion susceptibility of Mg–10Gd–2Y–0.5Zr, AZ91D alloy and pure magnesium using stochastic model". In: *Corrosion Science* 50.12 (Dec. 2008), pp. 3500–3507. DOI: 10.1016/j.corsci.2008.09.033. URL: https://doi.org/10.1016/j.corsci.2008.09.033.

[43] Jelena Perić, Ruža Krstulović, and Marijan Vučak. "Investigation of dehydroxylation of gibbsite into boehmite by DSC analysis". In: *Journal of thermal analysis* 46.5 (1996), pp. 1339–1347.

[44] Boquan Zhu, Binxiang Fang, and Xiangcheng Li. "Dehydration reactions and kinetic parameters of gibbsite". In: *Ceramics International* 36.8 (2010), pp. 2493–2498.

[45] Digby D Macdonald. "The point defect model for the passive state". In: *Journal of the Electrochemical Society* 139.12 (1992), p. 3434.

[46] Stuart Coles et al. *An introduction to statistical modeling of extreme values*. Vol. 208. Springer, 2001.

[47] Robert E. Melchers. "Extreme value statistics and long-term marine pitting corrosion of steel". In: *Probabilistic Engineering Mechanics* 23.4 (Oct. 2008), pp. 482–488. DOI: 10.1016/j.probengmech.2007.09.003. URL: https://doi.org/10.1016/j.probengmech.2007.09.003.

[48] T. Shibata. "1996 W.R. Whitney Award Lecture:Statistical and Stochastic Approaches to Localized Corrosion". In: *CORROSION* 52.11 (Nov. 1996), pp. 813–830. DOI: 10.5006/1.3292074. URL: https://doi.org/10.5006/1.3292074.

[49] Jin-Ju Park and Su-Il Pyun. "Stochastic approach to the pit growth kinetics of Inconel alloy 600 in Cl- ion-containing thiosulphate solution at temperatures 25–150 °C by analysis of the potentiostatic current transients". In: *Corrosion Science* 46.2 (Feb. 2004), pp. 285–296. DOI: 10.1016/s0010-938x(03)00158-6. URL: https://doi.org/10.1016/s0010-938x(03)00158-6.

[50] Zohreh Soltani Asadi and Robert E. Melchers. "Extreme value statistics for pitting corrosion of old underground cast iron pipes". In: *Reliability Engineering and System Safety* 162 (June 2017), pp. 64–71. DOI: 10.1016/j.ress.2017.01.019. URL: https://doi.org/10.1016/j.ress.2017.01.019.

[51] Jing Liu et al. "Modeling of the Critical Pitting Temperature between the Laboratory-Scale Specimen and the Large-Scale Specimen". In: *Journal of The Electrochemical Society* 165.7 (2018), pp. C328–C333. DOI: 10.1149/2.0521807jes. URL: https://doi.org/10.1149/2.0521807jes.

[52] P Prescott and AT Walden. "Maximum likelihood estimation of the parameters of the generalized extreme-value distribution". In: *Biometrika* 67.3 (1980), pp. 723–724.

[53] P Prescott and AT Walden. "Maximum likeiihood estimation of the parameters of the three-parameter generalized extreme-value distribution from censored samples". In: *Journal of Statistical Computation and Simulation* 16.3-4 (1983), pp. 241–250.

[54] Huynh Ngoc Phien and Tsu-Shang Emma Fang. "Maximum likelihood estimation of the parameters and quantiles of the general extreme-value distribution from censored samples". In: *Journal of Hydrology* 105.1-2 (Jan. 1989), pp. 139–155. DOI: 10.1016/0022-1694(89)90100-5. URL: https://doi.org/10.1016/0022-1694(89)90100-5.

[55] J. Maciunas Landwehr, N. C. Matalas, and J. R. Wallis. "Probability weighted moments compared with some traditional techniques in estimating Gumbel Parameters and quantiles". In: *Water Resources Research* 15.5 (Oct. 1979), pp. 1055–1064. DOI: 10.1029/wr015i005p01055. URL: https://doi.org/10.1029/wr015i005p01055.

[56] Huynh Ngoc Phien. “A review of methods of parameter estimation for the extreme value type-1 distribution”. In: *Journal of Hydrology* 90.3-4 (Apr. 1987), pp. 251–268. DOI: 10.1016/0022-1694(87)90070-9. URL: https://doi.org/10.1016/0022-1694(87)90070-9.

[57] Smail Mahdi and Myrtene Cenac. “Estimating Parameters of Gumbel Distribution using the Methods of Moments, probability weighted Moments and maximum likelihood”. In: *Revista de Matematica: Teoria y Aplicaciones* 12.1-2 (2005), pp. 151–156.

[58] Theodore W Anderson and Donald A Darling. “Asymptotic theory of certain ”goodness of fit” criteria based on stochastic processes”. In: *The annals of mathematical statistics* (1952), pp. 193–212.

[59] Hongjoon Shin et al. “Assessment of modified Anderson–Darling test statistics for the generalized extreme value and generalized logistic distributions”. In: *Stochastic Environmental Research and Risk Assessment* 26.1 (Apr. 2011), pp. 105–114. DOI: 10.1007/s00477-011-0463-y. URL: https://doi.org/10.1007/s00477-011-0463-y.